Catalysis Today 142 (2009) 308–313

Contents lists available at ScienceDirect

Catalysis Today

journal homepage: www.elsevier.com/locate/cattod

Study of ruthenium supported on Ta_2O_5–ZrO_2 and Nb_2O_5–ZrO_2 as catalysts for the partial oxidation of methane

Valerio Choque, Narcís Homs, Renata Cicha-Szot [1], Pilar Ramírez de la Piscina *

Department of Inorganic Chemistry and Institute of Nanoscience and Nanotechnology, Universitat de Barcelona, C/Marti i Franquès 1-11, 08028 Barcelona, Spain

ARTICLE INFO

Article history:
Available online 30 October 2008

Keywords:
Partial oxidation of methane
Ta_2O_5–ZrO_2 support
Nb_2O_5–ZrO_2 support
Supported Ru catalyst

ABSTRACT

Ru-based catalysts supported on Ta_2O_5–ZrO_2 and Nb_2O_5–ZrO_2 are studied in the partial oxidation of methane at 673–873 K. Supports with different Ta_2O_5 or Nb_2O_5 content were prepared by a sol–gel method, and $RuCl_3$ and $RuNO(NO_3)_3$ were used as precursors to prepare the catalysts (ca. 2 wt.% Ru). At 673 K high selectivity to CO_2 was found. An increase of temperature up to 773 K produced an increase in the selectivity to syngas (H_2/CO = 2.2–3.1), and this is related with the transformation of RuO_2 to metallic Ru as was determined from XRD and XPS results. At 873 K and with co-fed CO_2 an increase of the catalytic activity and CO selectivity was found. A TOF value of 5.7 s^{-1} and H_2/CO ratio ca. 1 was achieved over Ru(Cl)/6TaZr. Catalytic results are discussed as a function of the support composition and characteristics of Ru-based phases.

1. Introduction

The catalytic partial oxidation of methane (CPOM) can be regarded as a promising route for the production of synthesis gas which is used as feedstock in many important industrial processes [1–7]:

$$CH_4 + \tfrac{1}{2}O_2 \rightarrow CO + 2H_2 \quad \Delta H_{298} = -35.7\,kJ/mol$$

This process is more energy efficient than the highly endothermic methane steam reforming reaction. Noble metal catalysts have been studied in the CPOM reaction due to their high activity and small sensitivity to carbon deposition. It is generally agreed that Rh, Ir and Ru provide the best performances among other noble metals, in terms of H_2 and CO yields and the performance of these metals in the CPOM reaction strongly depends on the oxide used as support. Among other factors, the capability of surface oxygen exchange and the reducibility of the oxide can highly determine the catalytic behavior of the material. A high capability to provide and store oxygen could favors methane complete combustion resulting a low CPOM selectivity [8]. In general, reducible-oxides-supported rhodium catalysts show lower activities and selectivities than those supported on irreducible oxides [9]. However, Ru/TiO_2 catalysts show high selectivity to synthesis gas in the low methane conversion range at 873–973 K. It has been proposed that TiO_2 inhibits the oxidation of ruthenium under conditions of partial oxidation of methane and that a direct conversion reaction schema takes place over this system [3,10]. On the other hand, over Ir-based catalysts the activity of ZrO_2-supported catalysts in the CPOM has been reported to be similar to that of TiO_2-supported catalysts [11]. In order to explore new catalytic systems for the CPOM, we report the behavior in the partial oxidation of methane, of new ruthenium catalysts supported on binary systems based on Ta_2O_5–ZrO_2 and Nb_2O_5–ZrO_2; both pure Ta_2O_5 and pure Nb_2O_5 have a low surface oxygen exchange rate [12]. Although the characteristics of Ta_2O_5–ZrO_2 and Nb_2O_5–ZrO_2 mixed systems have been deeply studied as a function of the composition [13–15], their use as supports in the CPOM has not been reported. In this work the influence on the catalytic behavior of both the Ta and Nb content and the ruthenium precursor used in the preparation of catalysts is studied. We also explore the catalytic behavior of these new materials under CPOM with co-fed CO_2.

2. Experimental

Ta_2O_5–ZrO_2 binary materials were prepared by a sol–gel method using alcoxide compounds of tantalum and zirconium as reported previously [13]. Nb_2O_5–ZrO_2 materials were prepared in a similar manner using a propanol solution of $Nb(CH_3CH_2O)_5$. Solids were calcined at 873 K and labeled *x*TaZr and *x*NbZr, where *x* accounts for the w/w (%) of Ta_2O_5 and Nb_2O_5, respectively. The

* Corresponding author. Tel.: +34 934037056; fax: +34 934907725.
E-mail address: pilar.piscina@qi.ub.es (P.R. de la Piscina).
[1] Present address: Oil and Gas Institute, Department of Petroleum Engineering, Krakow, Poland.

0920-5861/$ – see front matter © 2008 Elsevier B.V. All rights reserved.
doi:10.1016/j.cattod.2008.09.013

supports were impregnated by the incipient wetness method using aqueous solutions of $Ru(NO)(NO_3)_3$ or $RuCl_3$ to obtain ca. 2% (w/w) of Ru in the catalyst and samples were labeled Ru(NO)/support and Ru(Cl)/support, respectively. The impregnated samples were dried at 373 K and calcined at 573 K.

The chemical composition of the supports was determined by X-ray fluorescence analysis using a Phillips PW-2400 apparatus equipped with Uniquant v. 2.53 software. The content of ruthenium was analyzed by inductively coupled plasma (ICP) in a PerkinElmer 3200RL Optima spectrometer. For the ICP analysis, calcined samples were fused with NaOH and Na_2O_2 at 723 K and then, successively treated with concentrate HCl, *aqua regia*, and HF.

The BET surface area of the supports was determined by nitrogen adsorption at 77 K using a Micromeritics ASAP9000 instrument.

The temperature programmed reduction (TPR) profiles and CO chemisorption experiments were carried out using a Micromeritics AutoChem II Chemisorption Analyzer. For TPR experiments calcined samples were heated (10 K/min) with a 12.5% H_2/Ar mixture (50 mL/min) up to 623 K. The hydrogen consumption was measured by a thermal conductivity detector. CO chemisorption was determined at 308 K.

The X-ray powder diffraction (XRD) patterns were obtained using a Bragg-Brentano PANalytical X'Pert PRO MPD Alpha1 X-ray diffractometer with nickel-filtered Cu Kα1 radiation (λ = 0.15406 nm). The XRD profiles were collected in the 2θ angle between 20° and 100°, at the step width of 0.017° and by counting 50 s at each step. The diffraction patterns obtained were compared to the corresponding JCPDS files.

The X-ray photoelectron spectra (XPS) were obtained using a Sage HR (Specs GmbH) spectrometer equipped with an Al Kα X-ray exciting source calibrated using the Ag $3d_{5/2}$ line. The residual pressure in the analysis chamber was maintained below 10^{-8} Torr. The binding energies (BE) were referred to the C 1 s peak at 284.9 eV which gave BE values with an accuracy of ±0.1 eV. The Ru 3d, Ta 4d, Nb 3d, Zr 3d and Cl 2p atomic levels were analyzed. Residual chlorine was not detected in the samples studied.

Catalytic tests were performed under differential conditions in a stainless steel continuous fixed-bed microreactor with on-line GC analysis of products using a VARIAN STAR 3400 CX apparatus equipped with a *carboxan* 1000 column and on-line TCD and FID. Only CO and CO_2 were found as carbon containing products. The selectivity of H_2, CO and CO_2 was calculated in the basis of the molar percentage of each product evolved with respect to the total moles of products evolved (water excluded). The reaction conditions were: P_T = 4 bar, T = 673–873 K, GHSV = 6500 h^{-1}, $CH_4/O_2/He$ = 6/1/22 molar ratio. The catalysts were diluted with inactive SiC and placed in the reactor, and the temperature was raised under He flow up to 573 K; then, the reactant mixture was introduced and temperature increased at 10 K/min up to 673 K. The catalysts were kept at this temperature for 4 h and the temperature was subsequently increased up to 773 K and maintained for 4 h in the standard catalytic tests or 24 h in the long-time catalytic tests. Selected catalysts were tested at 873 K and with CO_2 co-feeding (2.5% and 5%, v/v) maintaining the GHSV and CH_4 and O_2 flows.

3. Results and discussion

Table 1 compiles the TaZr and NbZr supports prepared with different Ta or Nb content and their BET surface areas. For both *x*TaZr and *x*NbZr systems the BET surface-area increased with the Ta or Nb content.

The characteristics of *x*TaZr materials have already been reported [13]. Briefly, the XRD patterns of 6TaZr and 22TaZr indicate the presence of crystalline monoclinic and tetragonal ZrO_2; the intensity of peaks characteristic of the tetragonal phase increases with the tantalum content. Diffraction peaks cannot be distinguished from the XRD pattern of 75TaZr and pure Ta_2O_5, probably because of the presence of large amounts of amorphous Ta_2O_5. From the XRD pattern of 9NbZr only the presence of crystalline tetragonal zirconia can be deduced. 25NbZr and 28NbZr supports with higher Nb content also show peaks which can be assigned to tetragonal zirconia, and others corresponding to the orthorhombic $Nb_2Zr_6O_{17}$ crystalline phase. Pure Nb_2O_5 was obtained as the orthorhombic phase.

Table 1
Ta_2O_5 or Nb_2O_5 content of supports and BET surface area.

Support	Ta_2O_5 or Nb_2O_5 (%, w/w)	BET (m^2/g)
ZrO_2	–	33
6TaZr	5.6	41
22TaZr	22.0	64
75TaZr	74.6	95
Ta_2O_5	–	75
9NbZr	8.8	10
25NbZr	25.2	40
28NbZr	28.0	86
Nb_2O_5	–	24

The XRD patterns of calcined catalysts after Ru impregnation did not show significant changes with respect to those of the corresponding supports. For samples with low Ta content, the presence of crystalline RuO_2 could not be determined because the peaks of monoclinic ZrO_2 would mask those of RuO_2. Contrariwise, the XRD patterns of Ru/75TaZr and Ru/Ta_2O_5, in which no peaks corresponding to the support can be distinguished, allowed to determine the presence of crystalline RuO_2 because of the presence of a peak at 2θ = 54.2° assigned to the most intense reflection (2 1 1) of the RuO_2 phase. The particle size determined using the Scherrer equation appears in Table 2, with values of 21–26 nm being obtained; significant differences of crystallite size of RuO_2 were not determined as a function of precursors used in the preparation of catalysts.

The XRD patterns of Ru/9NbZr and Ru/Nb_2O_5 catalysts do not show peaks corresponding to the RuO_2 phase. On the other hand, although the XRD pattern of Ru/25NbZr or Ru/28NbZr showed a peak at 2θ = 54.2° assigned to the (2 1 1) reflection of the RuO_2 phase, the presence of a peak at 2θ = 53.7° due to the (2 1 2) reflection of the orthorhombic $Nb_2Zr_6O_{17}$ crystalline phase, makes it difficult to determine the mean particle size of RuO_2 using the Scherrer equation in these cases.

Although the catalytic behavior of catalysts was determined after the calcination step, TPR experiments were carried out because the reduction state of Ru active phase can determine the catalytic behavior of Ru-based catalysts. Figs. 1 and 2 show the TPR profile of catalysts supported on xTaZr and xNbZr samples, respectively. In all cases ca. 2 mol H_2/mol Ru in the catalyst were consumed, indicating the total reduction of RuO_2. The reduction profiles of supported Ru catalysts depended on the support (*x*TaZr or *x*NbZr) and on the ruthenium precursor used in their preparation; hydrogen consumption peaks between 400 and 445 K, assigned to the reduction of well-dispersed RuO_x and RuO_2 particles were found. In general, for the same precursor, the *x*NbZr-supported catalyst is reduced at lower temperature than the *x*TaZr-supported catalyst. On the other hand, great differences in the reducibility properties were found for catalysts with low Ta content and Ru/ZrO_2 prepared from $RuCl_3$ or $RuNO(NO_3)_3$ precursors; catalysts prepared from $RuCl_3$ are reduced at lower temperature. However, for TaZr-supported catalysts with high content of Ta, broad peaks displaced at higher temperatures were obtained when ruthenium chloride was used as precursor in

Table 2
Ruthenium content of catalysts (%, w/w) determined by chemical analysis.

Sample	%Ru	*d* RuO_2 DRX (nm)	*d* Ru* DRX (nm)	*d* Ru* (CO) (nm)	*d* Ru** XRD (nm)	*d* Ru** (CO) (nm)
$Ru/(NO)ZrO_2$	2.3	[a]	17	15	13	–
Ru(NO)/6TaZr	2.2	[a]	14	17	16	28
Ru(NO)/22TaZr	2.2	[a]	19	21	20	–
Ru(NO)/75TaZr	2.1	26	17	22	20	30
$Ru(NO)/Ta_2O_5$	2.3	21	24	27	14	–
Ru(NO)/9NbZr	1.8	n.d.	–	23	22	–
Ru(NO)/25NbZr	2.0	[a]	–	25	23	–
Ru(NO)/28NbZr	1.9	[a]	–	27	27	–
$Ru(NO)/Nb_2O_5$	2.0	n.d.	–	37	28	–
$Ru(Cl)/ZrO_2$	1.4	[a]	–	11	12	–
Ru(Cl)/6TaZr	1.5	[a]	–	15	10	20
Ru(Cl)/22TaZr	1.5	[a]	–	11	11	–
Ru(Cl)/75TaZr	1.5	24	–	25	18	25
$Ru(Cl)/Ta_2O_5$	1.4	23	–	25	22	–
Ru(Cl)/9NbZr	1.5	n.d.	25	20	17	25
Ru(Cl)/25NbZr	1.5	[a]	–	22	20	–
Ru(Cl)/28NbZr	1.5	[a]	20	23	26	27
$Ru(Cl)/Nb_2O_5$	1.4	n.d.	–	26	30	–

Mean crystallite size of RuO_2 determined by Scherrer equation in calcined catalysts. Mean crystallite size of Ru particles after the TPR experiments* or catalytic test at 773 K**, determined from DRX or CO chemisorption.
[a] Peaks of RuO_2 may be masked by the peaks of the support or they are located close to them. (n.d.) Peaks of RuO_2 were not detected.

the preparation of catalysts. A strong interaction between the Ru species and the amorphous support could be proposed in these cases. After the TPR experiments carried out at temperatures up to 623 K, the chemisorption of CO was performed at 308 K and the corresponding mean particle size was calculated assuming a stoichiometry CO:Ru 1:1 and spherical shape of Ru particles. Results of particle size appear in Table 2. In general, catalysts prepared from $RuCl_3$ show lower particle size than their homologues prepared from $RuNO(NO_3)_3$. The lowest particle size is shown by the catalysts prepared from $RuCl_3$ and supported on ZrO_2 or supports with low Ta content (6TaZr, 22TaZr). In some cases the estimation of the crystallite size was done by the Scherrer equation from the XRD patterns of catalysts obtained after the TPR experiment. In general a good concordance between both results was obtained.

After the calcination step at 573 K, catalysts were tested in the CPOM reaction, and they were characterized by XRD, CO chemisorption and XPS after reaction at 773 K. The XRD patterns of post-reaction samples are depicted in Figs. 3–6. In all cases, besides the diffraction peaks of the support, a peak at $2\theta = 44.0^\circ$ appeared. This peak can be assigned to the most intense reflection (1 0 1), of the Ru_{hcp} phase. For 75TaZr- and Ta_2O_5-supported catalysts, the crystalline RuO_2, if present, could be evidenced by DRX, as discussed above. The absence of a peak at $2\theta = 54.2^\circ$ which was visible in the XRD pattern of calcined catalysts, accords with the reduction of RuO_2 under reaction conditions. Catalysts Ru(Cl)/6TaZr, Ru(NO)/6TaZr, Ru(Cl)/9NbZr and Ru(Cl)/28NbZr were analyzed by XPS after the calcination step and before the catalytic test. In all cases, the BE corresponding to the Ru $3d_{5/2}$ level was 280.5–280.6 eV, which indicated the presence of oxidized ruthenium (RuO_2). The Ru(Cl)/6TaZr was analyzed after reaction by XPS, and a Ru $3d_{5/2}$ BE of 279.5 eV was obtained, which is characteristic of metallic ruthenium and similar to that obtained for the same catalyst after reduction at 723 K (279.5 eV). The transformation of RuO_2 phase to Ru under reaction conditions, which has been evidenced by XRD and XPS can be related with the reaction:

$$CH_4 + 2RuO_2 \rightarrow CO_2 + 2Ru + 2H_2O$$

In accordance with the easy reducibility of catalysts shown by TPR experiments, this reaction, which has been proposed to occur in supported Ru catalysts under CPOM reaction conditions, would be responsible for the formation of metallic ruthenium and thus for the activation of catalysts that increase their activity in the CPOM reaction [16,17].

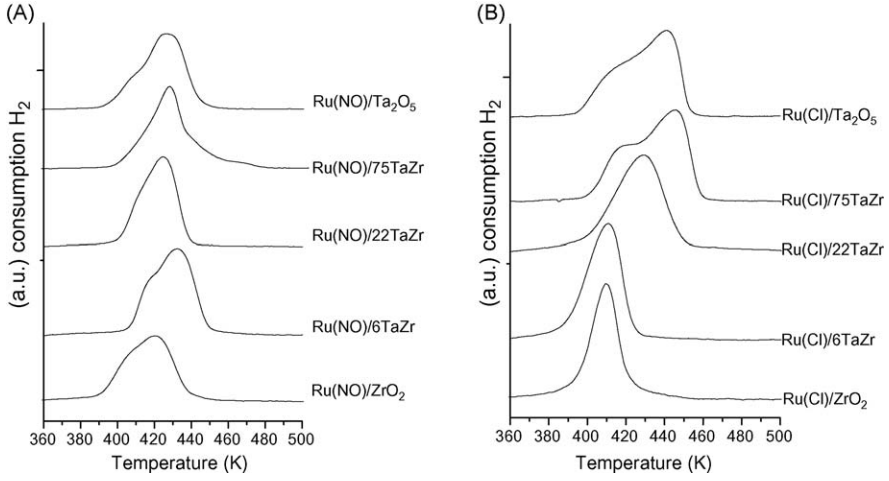

Fig. 1. H_2-TPR of the Ru/*x*TaZr catalysts prepared from different Ru precursors: (A) $RuNO(NO_3)_3$; (B) $RuCl_3$.

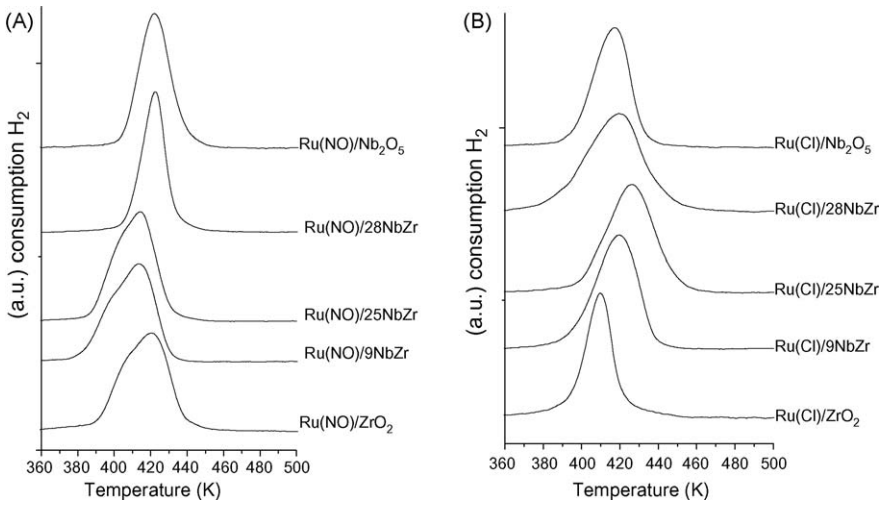

Fig. 2. H_2-TPR of the Ru/*x*NbZr catalysts prepared from different Ru precursors. (A) $RuNO(NO_3)_3$; (B) $RuCl_3$.

From the XRD patterns the Ru crystallite size of the used catalysts was estimated using the Scherrer equation; in several cases the particle size was also determined by CO chemisorption. For both Nb_2O_5–ZrO_2- and Ta_2O_5–ZrO_2-supported catalysts, an increase of Ru particle size with the increase of Nb or Ta content of the support was determined. Results are compiled in Table 2. In general, results of particle size determined by CO chemisorption of post-reaction catalysts were higher than those obtained by XRD; only in the case of Ru(Cl)/28NbZr, which showed a high particle size, were similar values determined by XRD and CO chemisorption. The mean particle size determined from CO chemisorption and the crystallite size estimated from XRD analysis of reduced catalysts were within the experimental error in good agreement. The differences found between the results obtained for post-reaction catalysts may be interpreted in terms of formation of aggregates of Ru crystallites, by the partial decoration of the Ru particles with species coming from the support and/or by carbon deposition in ruthenium-active sites.

Catalysts were active in the partial oxidation of methane. H_2, CO and CO_2 were the products obtained. At 673 K, in all cases, high selectivity to CO_2 was obtained because of the presence of RuO_2 which catalyses the methane total oxidation:

$$CH_4 + 2O_2 \rightarrow CO_2 + 2H_2O$$

At 773 K and CH_4 conversion values of ca. 15–20%, H_2/CO ratios of 2.2–3.1 were obtained, as a function of support used. In general, for Ru/*x*TaZr and Ru/*x*NbZr catalysts, the activity of catalysts per mole of Ru was higher for catalysts prepared from $RuCl_3$ in comparison with that of catalysts prepared from $RuNO(NO_3)_3$; this can be related with the smaller particle size of Ru^0 observed after reaction for the Ru(Cl)/support catalysts (Table 2). On the other hand, the catalytic activity of Ru(NO)/*x*TaZr and Ru(NO)/*x*NbZr systems was higher than those of Ru(NO)/ZrO_2, Ru(NO)/Nb_2O_5 or Ru(NO)/Ta_2O_5 catalysts. Among Ru/*x*TaZr systems, the Ru/6TaZr catalyst showed the highest catalytic activity (Table 3). In the 6TaZr support, besides monoclinic and tetragonal ZrO_2, surface tantalum species exist, being the Ta coverage below the monolayer (the monolayer value for these materials is ca. 20%, w/w, Ta_2O_5 [13]). Catalysts in which the presence of amorphous Ta_2O_5 has been proposed (Ru/75TaZr and Ru/Ta_2O_5) showed a high CO_2 selectivity. With respect to the Ru/*x*NbZr series, catalysts with 28% (w/w) Nb_2O_5 content showed the highest syngas yield and the lowest CO_2 selectivity values; the support of these catalysts was constituted by tetragonal ZrO_2 and the crystalline mixed phase $Nb_2Zr_6O_{17}$.

For the catalysts for which the CO chemisorption experiments were carried out, the exposed Ru was determined and the turnover

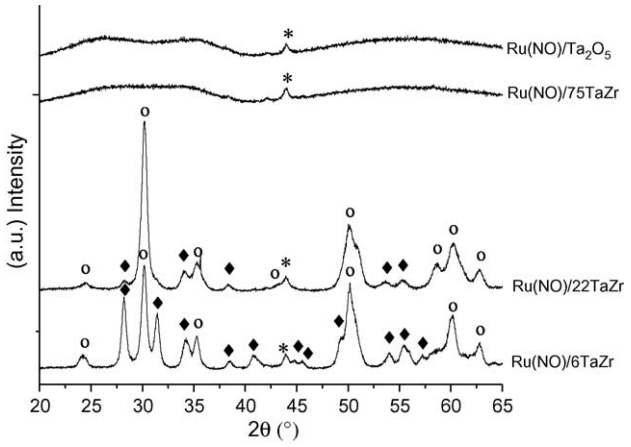

Fig. 3. XRD patterns of Ru(NO)/*x*TaZr post-reaction samples. *, Ru_{hcp}; ○, ZrO_2 tetragonal; ◆, ZrO_2 monoclinic.

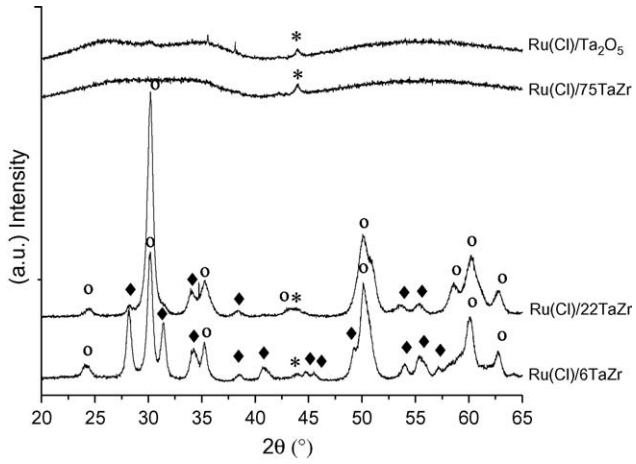

Fig. 4. XRD patterns of Ru(Cl)/*x*TaZr post-reaction samples. *, Ru_{hcp}; ○, ZrO_2 tetragonal; ◆, ZrO_2 monoclinic.

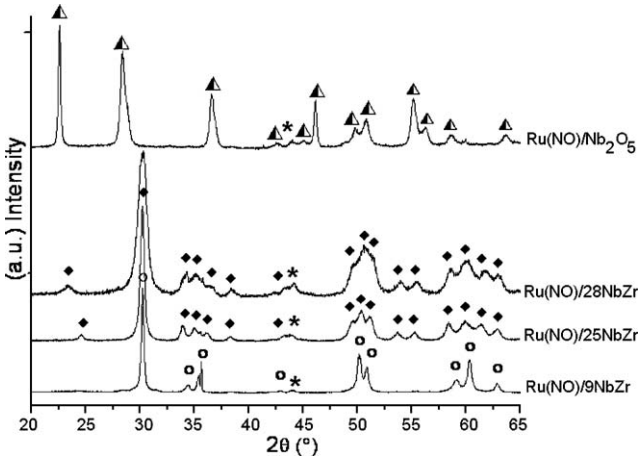

Fig. 5. XRD patterns of Ru(NO)/*x*NbZr post-reaction samples. *, Ru_{hcp}; ○, tetragonal ZrO_2; ◆, orthorhombic $Nb_2Zr_6O_{17}$; ◭, orthorhombic Nb_2O_5.

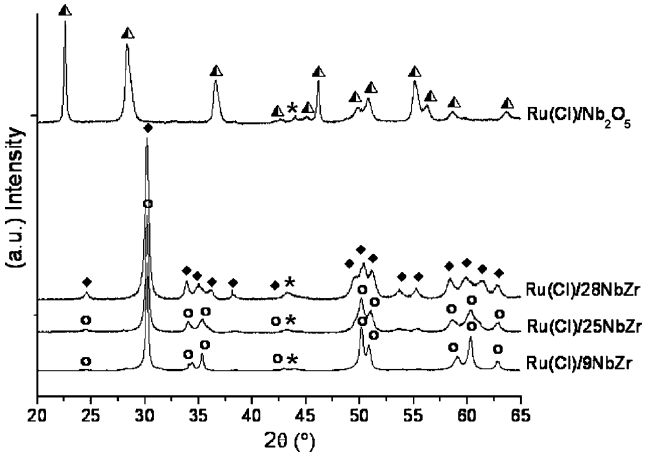

Fig. 6. XRD patterns of Ru(Cl)/*x*NbZr post-reaction samples. *, Ru_{hcp}; ○, tetragonal ZrO_2; ◆, orthorhombic $Nb_2Zr_6O_{17}$; ◭, orthorhombic Nb_2O_5.

frequency number (TOF) referred to methane transformed, was calculated. Values in the range 2.1–2.8 s^{-1} were obtained (Table 3).

The stability of one representative catalyst of each series, Ru(Cl)/6TaZr and Ru(Cl)/28NbZr, was tested in a longer reaction time. Fig. 7 shows conversion values and product distribution. Both Ru(Cl)/6TaZr and Ru(Cl)/28NbZr show a catalytic behavior almost unchanged over 24 h.

On the other hand, two catalysts were selected to study their catalytic behavior at higher temperature (873 K) and with the co-feeding of CO_2. Fig. 8 shows the profiles of conversion and product

Table 3
Catalytic behavior of catalysts in the partial oxidation of methane after 4 h of reaction at 773 K.

Catalyst	CH_4 Conv (%)	Activity ($molCH_4/mol_{Ru}$ h)	TOF (s^{-1})	Selectivity (%)[a]			H_2/CO
				H_2	CO	CO_2	
Ru(NO)/ZrO_2	19	273		56.0	21.4	22.6	2.6
Ru(NO)/6TaZr	22	333	2.1	53.3	21.1	25.6	2.5
Ru(NO)/22TaZr	20	312		53.3	19.7	27.0	2.7
Ru(NO)/75TaZr	18	295	2.0	50.2	18.7	31.1	2.7
Ru(NO)/Ta_2O_5	16	248		49.7	16.0	34.3	3.1
Ru(NO)/9NbZr	18	336	2.3	51.6	17.6	30.8	2.9
Ru(NO)/25NbZr	20	340		50.8	21.6	27.6	2.4
Ru(NO)/28NbZr	20	352	2.8	50.2	23.3	26.5	2.2
Ru(NO)/Nb_2O_5	16	267		50.6	20.4	29.0	2.5
Ru(Cl)/ZrO2	22	472		53.7	19.9	26.4	2.7
Ru(Cl)/6TaZr	21	471	2.2	54.0	19.8	26.2	2.7
Ru(Cl)/22TaZr	17	374		56.2	20.9	22.9	2.7
Ru(Cl)/75TaZr	14	321	1.7	50.8	19.8	29.4	2.6
Ru(Cl)/Ta_2O_5	16	392		49.8	19.8	30.4	2.5
Ru(Cl)/9NbZr	19	459	2.1	54.4	21.4	24.2	2.5
Ru(Cl)/25NbZr	17	394		54.8	23.3	21.9	2.3
Ru(Cl)/28NbZr	20	456	2.4	55.7	23.5	20.7	2.4
Ru(Cl)/Nb_2O_5	16	375		51.0	19.9	29.1	2.6

[a] Molar percentage of products (water not included).

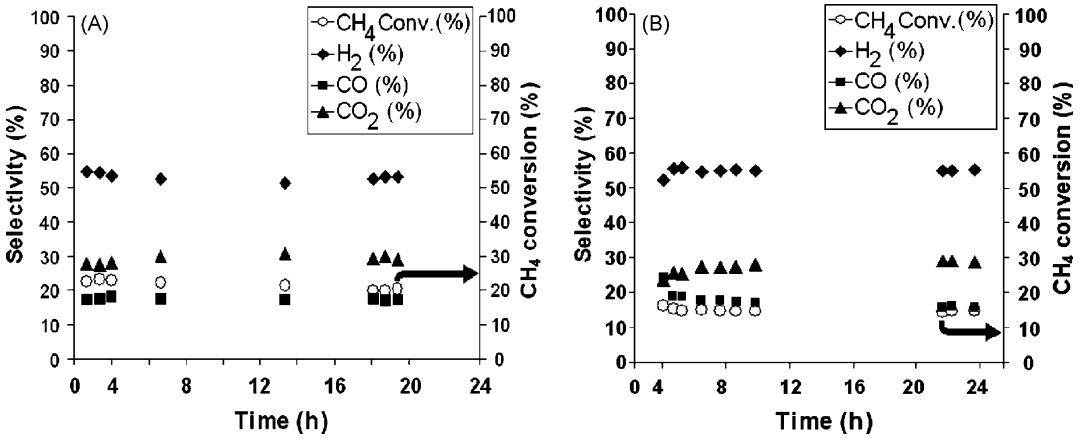

Fig. 7. Catalytic behavior of several catalysts at 773 K: (A) Ru(Cl)/6TaZr; (B) Ru(Cl)/28NbZr. P_T = 4 bar, GHSV = 6500 h^{-1}, $CH_4/O_2/He$ = 6/1/22 molar ratio.

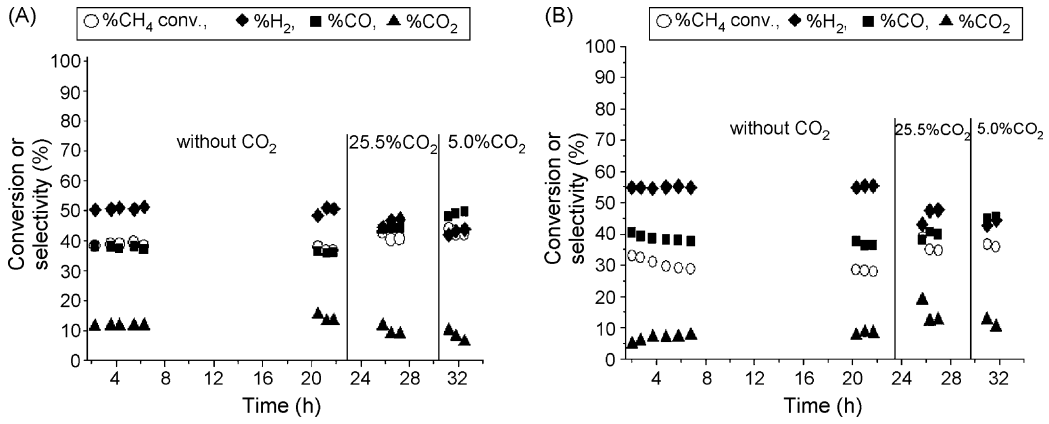

Fig. 8. Catalytic behavior of several catalysts at 873 K: (A) Ru(Cl)/6TaZr; (B) Ru(Cl)/9NbZr. Initial conditions: P_T = 4 bar, GHSV = 6500 h^{-1}, CH_4/O_2/He = 6/1/22 molar ratio. After 24 h of reaction, CO_2 was co-fed in the reactants, 2.5% (v/v) CO_2 and then 5% (v/v) CO_2.

distribution of Ru(Cl)/6TaZr and Ru(Cl)/9NbZr under these experimental conditions. The temperature increase from 773 to 873 K produced an increase in activity that was higher for Ru(Cl)/6TaZr. Moreover, the H_2/CO ratio decreased to H_2/CO = 1.3–1.5 values because the selectivity to CO_2 diminished and that to CO increased. Under these conditions, metallic ruthenium would be stabilized, the combustion of methane should be minimized and the reverse water gas shift reaction can occur. The CO_2 co-feeding (2.5–5%, v/v) in the reactant mixture produced an increase of activity and an ulterior decrease of H_2/CO ratio (H_2/CO = 0.9–1.2). A TOF of 4.6 s^{-1} for Ru(Cl)/9NbZr and 5.7 s^{-1} for Ru(Cl)/6TaZr were obtained using the CO chemisorption measurements carried out after the catalytic test at 873 K. The addition of CO_2 can tune the catalytic activity and/or the selectivity by tuning the catalyst surface characteristics under working conditions and/or favoring the occurrence of new or parallel reactions in which CO_2 could be involved, i.e. dry reforming and/or reverse of water gas shift reaction. The constant removal of CH*x* or carbonaceous surface species could account for an increase of activity and CO yield:

$$CHx + CO_2 \rightarrow 2CO + (x/2)H_2$$

4. Conclusions

Supported Ru/*x*TaZr and Ru/*x*NbZr systems are appropriate as catalysts for the CPOM at moderate temperature. The initial RuO_2 phase transforms under reaction conditions to the active Ru^0 phase, which is present in the catalysts after reaction at 773 K. The use of $RuCl_3$ as precursor in the preparation of catalysts leads to a lower particle size of Ru^0 than the use of $Ru(NO)(NO_3)_3$. When the CPOM was carried out at 673 K, in all cases high selectivity to CO_2 was encountered, and this is related with the presence of RuO_2 at this temperature and the role of support in the CH_4 oxidation. At 773 K, high selectivity to syngas (H_2/CO = 2.2–2.9) was obtained. A tantalum content in the support lower than monolayer values favors the CPOM, meanwhile for Ru/*x*NbZr catalysts an increase in niobium content up to ca. 30% (wt. Nb_2O_5) increases the yield in synthesis gas and produces catalysts which show higher TOF values. When reaction temperature is increased at 873 K, activity increases and lower H_2/CO ratios and CO_2 selectivity are obtained, and at this temperature the CO_2 addition has a positive effect on the catalytic behavior to yield syngas with a H_2/CO ratio of ca. 1.

Acknowledgements

The authors are grateful to Spanish and Catalan governments for financial support (research projects MAT2005-03456 and 2005SGR-00184, respectively). V. Choque acknowledges an AECI-MAE grant and R. Cicha-Szot the Erasmus exchange program between the University of Barcelona and the University of Science and Technology, AGH, Kraków.

References

[1] A.T. Ashcroft, A.K. Cheetham, J.S. Foord, N.M.L.H. Green, C.P. Grey, P.D.F. Vermont, Nature 344 (1990) 321.
[2] M.A. Peña, J.P. Gomez, J.L.G. Fierro, Appl. Catal. A: Gen. 144 (1996) 7.
[3] C. Elmasides, D.I. Kondarides, S.G. Neophytides, X.E. Verykios, J. Catal. 198 (2001) 195.
[4] T. Bruno, A. Beretta, G. Groppi, M. Roderi, P. Forzatti, Catal. Today 99 (2005) 89.
[5] J. Requies, M.A. Cabrero, V.L. Barrio, J.F. Cambra, M.B. Güemez, P.L. Arias, V. La Parola, M.A. Peña, J.L.G. Fierro, Catal. Today 116 (2006) 304.
[6] A.C.W. Koh, L. Chen, W.K. Leong, B.F.G. Johnson, T. Khimyak, J. Lin, Int. J. Hydrogen Energy 32 (2007) 725.
[7] R.M. Navarro, M.A. Peña, J.L.G. Fierro, Chem. Rev. 107 (2007) 3952.
[8] R. Lanza, S.G. Järas, P. Canu, Appl. Catal. A: Gen. 325 (2007) 57.
[9] E. Ruckenstein, H.Y. Wang, J. Catal. 187 (1999) 151.
[10] C. Elmasides, D.I. Kondarides, W. Grünert, X.E. Verykios, J. Phys. Chem. B 103 (1999) 5227.
[11] K. Nakagawa, N. Ikenaga, T. Suzuki, T. Kobayashi, M. Haruta, Appl. Catal. A: Gen. 169 (1998) 281.
[12] S.H. Taylor, J.S.J. Hargreaves, G.J. Hutchings, R.W. Joyner, Appl. Catal. A: Gen. 126 (1995) 287.
[13] B. Samaranch, P. Ramirez de la Piscina, G. Clet, M. Houalla, P. Gélin, N. Homs, Chem. Mater. 19 (2007) 1445.
[14] L.J. Buercham, J. Datka, I.E. Wachs, J. Phys. Chem. B 103 (1999) 6015.
[15] T. Onfroy, G. Clet, M. Houalla, J. Phys. Chem. B 109 (2005) 14588.
[16] S. Rabe, T.-B. Truong, F. Vogel, Appl. Catal. A: Gen. 292 (2005) 177.
[17] S. Rabe, M. Nachtegaal, F. Vogel, Phys. Chem. Chem. Phys. 9 (2007) 1461.